Catal Lett (2017) 147:2057–2066
DOI 10.1007/s10562-017-2088-3

Performance of Nickel Supported on γ-Alumina Obtained by Aluminum Recycling for Methane Dry Reforming

Ysla França Adans[1] · Adriana Daniela Ballarini[2] · André Rosa Martins[1] · Rodrigo Estevam Coelho[3] · Luciene Santos Carvalho[1]

Received: 20 January 2017 / Accepted: 22 May 2017 / Published online: 17 June 2017

Abstract In this paper, Ni/Al_2O_3 catalysts were prepared by using alumina synthesized from aluminum can powders, with or without ink. The catalysts produced were tested for methane dry reforming and showed not only high methane conversion (68–80%), but carbon dioxide (75–90%), selectivity to hydrogen (80–83%) as well as and H_2/CO molar ratio close to 1. Therefore, it is a promising idea for future industrial applications. The results also showed that contaminant metals present in aluminum cans could affect the catalysts properties.

Graphical Abstract

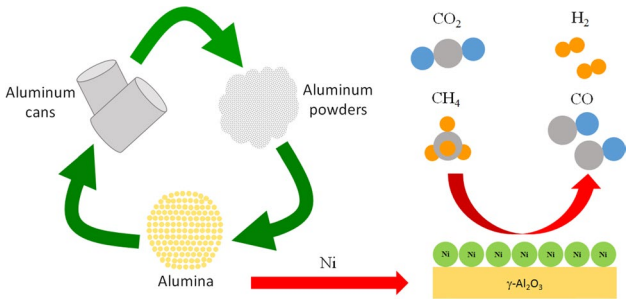

Keywords Alumina from recycling · Ni/Al_2O_3 · Dry reforming · Hydrogen · Syngas

1 Introduction

Biomass is an abundant and renewable source of energy. It is based on carbon, therefore it would be an alternative for petroleum usage and it can be processed in biorefineries to obtain fuels and chemicals [1]. Thus, biomass reforming is considered a sustainable technology that can be used in hydrogen and synthesis gas production and it been widely studied [2–7]. Its advantage in comparison to fossil fuels is based on the low emission of carbon dioxide and other gasses which are responsible for the greenhouse effect [1]. Besides, the carbon dioxide released from biomass gasification can be reused in processes such as photosynthesis, this not being possible with fossils fuels such as natural gas and oil. Through biomass gasification, a mixture of water, carbon oxides, methane and light hydrocarbons is produced. Water steam and carbon dioxide present in the mixture can act as oxidizing agents in processes such as methane steam reforming and methane dry reforming, respectively [2].

✉ Luciene Santos Carvalho
lusantos@ifba.edu.br

[1] Grupo de Pesquisa em Materiais e Catálise, Instituto Federal da Bahia, Campus Camaçari, Loteamento Espaço Alpha, s/n, BA 522, Limoeiro, Camaçari, BA 42802-590, Brazil

[2] Facultad de Ingeniería Química - FIQ, Instituto de Investigaciones en Catálisis y Petroquímica "Ing. José Miguel Parera" - INCAPE, Universidad Nacional del Litoral - UNL, CONICET, Colectora Ruta Nacional No 168, Km 0, Paraje El Pozo, 3000 Santa Fe, Argentina

[3] Grupo de Pesquisa em Processamento e Caracterização de Materiais, Instituto Federal da Bahia, Rua Emídio dos Santos, s/n, Barbalho, Salvador, BA 40301-015, Brazil

Hydrogen production for fuel cells from biogas reforming produced from biomass processing is very attractive, especially when organic waste is used as a feedstock. It contributes to reduce the waste accumulation, besides it would be a sustainable solution for energy generation [3]. In this reaction, a mixture of methane and carbon dioxide (biogas components) is converted into hydrogen and carbon monoxide (synthesis gas). The hydrogen produced can be used in fuel cells which only produce electricity, heat and water so that there is no environmental pollution. On the other hand, the synthesis gas with low H_2/CO molar ratio is suitable for liquid hydrocarbons production through Fischer–Tropsch process [8]. Therefore, biogas exploration is advantageous from both economic and environmental points of view [9].

Catalysts used for biogas dry reforming are typically based on nickel supported on alumina. Nickel is still the metal with the highest activity/cost ratio while alumina used as support provides thermal and mechanical resistance suitable to operational conditions and high specific surface area [10]. Many papers in the literature report the use of nickel/alumina catalysts in biogas dry reforming [9, 11, 12]. Rathod and Bhale [9], for instance, performed systematic investigation regarding spatial velocity effect, temperature and biogas composition on 10% Ni/Al_2O_3 catalysts performance for biogas reforming. They observed that the catalyst showed high conversion in all studied conditions and the equilibrium conversion was reached at 700 °C.

Alumina used as catalyst support can be obtained by different ways. One of them is the Bayer process which involves bauxite refining, the mineral from which alumina is extracted [13] and the sol–gel method, which is based on aluminum alkoxide hydrolysis or aluminum salt precipitation with ammonium hydroxide in controlled pH. Harmful compounds are released to the environment. Recently, it has been published that alumina can be prepared by precipitation reactions using aluminum powders from high-energy milling as raw material [14]. This approach is potentially interesting, not only due to economic and energetic considerations but also due to the social and ecological ones, which becomes another route for aluminum recycling. It avoids expenses related to bauxite extraction and its reduction to metal which requires high energy consumption. The results of this work showed that the gamma alumina produced in this way presented similar characteristics to commercial gamma alumina or the one synthesized by sol–gel method and therefore it could be used as catalyst support. Besides, the use of sodium hydroxide as precipitating agent was more advantageous than the use of ammonium hydroxide because it produces alumina with higher surface area and it do not release harmful substances into the environment [14].

In their tutorial review, Balakrishnam et al. [15] pointed several large scale wastes which can be used for catalytic purposes, such as red mud, aluminum dross, fly ash, slag from iron manufacture, chicken egg shells and rice husk ash. According to these authors, the use of waste materials as low-cost sources to obtain active catalytic systems or precursors for catalysts synthesis have caught on, especially for economic and environmental reasons. These authors also commented about publications involving the slag application as aluminum source for catalytically active materials preparation. However, no reports were found in literature about the use of aluminum cans to produce supports or catalysts based on alumina.

Based on these aspects, the aim of this work is to verify the γ-alumina usage feasibility, prepared from aluminum powders obtained through aluminum cans high-energy milling as described in [14], as a catalyst support. Thus, considering that nickel is still the most active phase in methane reforming catalysts, catalytic systems based on nickel supported on γ-alumina from aluminum recycling were prepared and characterized in this paper. Catalyst properties were evaluated by X-ray diffraction, X-ray fluorescence, nitrogen adsorption measurements, scanning electron microscopy, temperature-programmed reduction and cyclohexane dehydrogenation while its catalytic performance was measured for methane reforming with carbon dioxide or methane dry reforming (with reagent composition approximately equal to that of biogas). Catalytic systems prepared from recycled aluminum powders alumina were compared with the ones based on nickel supported on γ-alumina prepared by a conventional sol–gel method. The ink presence effect from aluminum cans powders used in alumina preparation on the catalysts properties and performance was investigated too.

2 Experimental

2.1 Catalysts Preparation

The supports were produced from reaction of aluminum powders obtained from aluminum cans high-energy milling (1000 rpm, 1 h) using a horizontal attritor mill, designed and assembled by Coelho [16], with HCl and, after, with NaOH. The procedure had been previously reported [14]. According to this method, aluminum powders were weighed in a beaker and after water addition reacted with hydrochloric acid solution, dropwise, under constant stirring, producing aluminum chloride ($AlCl_3$). Aluminum chloride was then converted into aluminum hydroxide by reaction with sodium hydroxide solution. After 24-h maturation, the mixture was separated by centrifugation and the solid was washed with ammonium hydroxide solution. The

gel obtained was dried, crushed, sieved (100–200 mesh) and calcined at 800 °C for 4 h. Alumina was obtained from aluminum can powders with ink (AS-T) and without ink (AS), besides the one prepared by the conventional sol–gel route (AC) [14], was impregnated with 10 wt% Ni, using 2.0 ml nickel nitrate aqueous solution (Sigma-Aldrich, 98.5%) per gram of support. The solvent was evaporated by heating at 70 °C in water bath. After impregnation, solids were dried at 110 °C (24 h) and calcined in air at 600 °C (4 h). The obtained samples were named AS-T 10N, AS 10N and AC 10N.

2.2 Catalysts Characterization

X-ray diffractograms (XRDs) were obtained in a Shimadzu XRD 6000. During the experiments, the samples were exposed to CuKα (1.54 Å) radiation, generated at 40 kV and 30 mA. The scan ranged from 10° to 80°. The chemical composition of calcined materials was determined by X-ray fluorescence (XRF) on a Shimadzu EDX-720. Scanning electron microscopy (SEM) images of the calcined samples were also obtained in a TESCA VEGA 3 at 15 kV. The specific surface areas (Sg) and pore volumes (Vp) were determined by nitrogen adsorption measurements in a ASAP 2020, using 200–300 mg sample. The specific surface area was determined by Brunauer-Emmett-Teller (BET) method while pore volume was determined by single point method. Besides, temperature-programmed reduction (TPR) analyses were carried out in a Quantachrome CHEMBET 3000. Before the experiment, samples (80 mg) were pre-treated at 100 °C for 1 h under N_2 flow and then they were heated from 30 to 1000 °C under 5% H_2/N_2 flow. Moreover, the metallic phase was characterized by cyclohexane dehydrogenation (CHD) test reaction, which was carried out in a differential reactor with H_2/CH molar ratio = 26, 20 mg sample, 1 atm and 300 °C. Before the test, the solids were reduced at 700 °C for 2 h under hydrogen flow. The reactor effluent was analyzed by using on-line chromatographic system with flame ionization detector (FID) with Cromosorb column. The activation energy values were determined from ln R^o curve slope as a function of 1/T[K] and R^o (reaction rate) was calculated from the conversion values obtained at three different temperatures.

2.3 Catalysts Evaluation

The different catalysts were tested in methane dry reforming (MDR) reaction that was carried out in a continuous-flow equipment at 700 °C, 1 atm for 5 h. Before the tests, samples (0.05 g) were reduced, in situ, at 700 °C for 2 h under H_2 flow. After that, the CH_4/CO_2 mixture (CH_4/CO_2 molar ratio = 1) was fed to the reactor at 20 ml min^{-1}. In order to avoid diffusional effects, catalyst particle sizes were very small (<80 mesh). Reactants and reaction products were analyzed by using online chromatographic system (GC–TCD) containing a Supelco Carboxen 1006 PLOT (30 m x 0.53 mm) column.

3 Results and Discussion

3.1 XRD

In the XRD pattern of aluminum can powders with ink (AL-T sample), showed in Fig. 1a, only four strong diffraction peaks were identified at 2θ with values 38.5°, 44.8°, 65.2° and 78.2°, corresponding to crystalline plans (111), (200), (220) and (311), respectively, which are characteristic of metallic aluminum (JCPDS 89-4037 card). After chemical reactions used to produce alumina precursors from aluminum powders, as described in [14], the diffraction peaks observed in AL-T were modified, giving new patterns for AS NC and AS-T NC samples (NC means non-calcined), as it can be seen in Fig. 1a. AS-T NC and AS NC XRD profiles were very similar. Besides the peaks related to the boehmite phase formation, AlOOH (JCPDS 21-1307 card), peaks corresponding to sodium chloride, NaCl (JCPDS 05-0628 card) were shown, which is an undesirable byproduct. However, after washing procedure, NaCl was eliminated from the solids that, after calcination, showed γ-Al_2O_3 phase characteristic profiles (JCPDS 29-0063 card), as it can be seen from XRD patterns of AS and AS-T samples in Fig. 1b. This phase was found when alumina was prepared by conventional sol–gel method (AC). Therefore, through XRD analysis, it was possible to verify γ-alumina formation from aluminum can powders. It was also noted that the diffraction peaks were more intense for AS-T NC and AS-T samples, compared to AS NC and AS samples, indicating that the crystallinity degree was higher for materials containing ink.

The XRD patterns of impregnated samples (Fig. 1c) indicated that nickel addition formed NiO (JCPDS 71-1179 card) and a nickel aluminate spinel structure, $NiAl_2O_4$ (JCPDS 10-0339 card), which could result from the strong interaction between NiO and γ-Al_2O_3. This is in agreement with results of Asencios et al. [17]. In fact, the diffraction peaks at 2θ values near 37°, 46° and 66° for the three patterns could correspond to the presence of both $NiAl_2O_4$ spinel phase and γ-Al_2O_3 pseudo-spinel phase whose network structure characteristics resemble $NiAl_2O_4$ ones [18, 19]. Since both crystallographic planes show the same Bragg angles (2θ), the peaks superposition occurs [17], as observed in XRD patterns. Regarding AC 10N, it was also hard to distinguish the NiO characteristic peaks due to the overlap with $NiAl_2O_4$ and γ-alumina peaks, as other authors reported [20]. It suggests that NiO could be segregated in

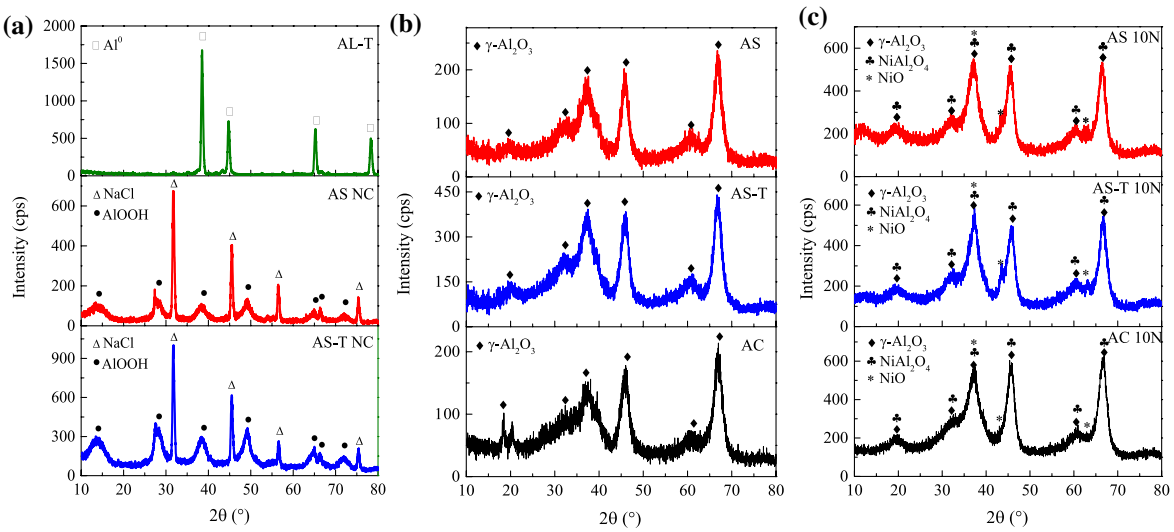

Fig. 1 XRD patterns: **a** aluminum cans powders with ink (AL-T) and precursors obtained from aluminum cans powders without ink (AS NC) and with ink (AS-T NC); **b** supports obtained from aluminum cans powders without ink (AS) and with ink (AS-T) and by conventional method (AC); **c** supports impregnated with 10 wt% Ni

this sample and in interaction with γ-alumina, because of the increase of the diffraction peaks magnitude, at 2θ with values 37.1°, 45.7° and 66.7° for AC 10N. Compared with AS 10N and AS-T 10N, the highest nickel amount would be correspond to nickel aluminate spinel, as pointed out by Luna and Iriarte [21]. On the other hand, NiO peaks (at 2θ with values 43.4° and 62.3°) were more defined and intense in AS-T 10N sample profile. Probably, a higher amount of segregated NiO was produced in that sample [17].

3.2 XRF

The chemical composition of aluminum can powders with ink (AL-T sample) was determined by XRF and the results are shown in Table 1. It was observed that, apart from aluminum, other elements such as magnesium, manganese, iron, potassium, and silicon could be found. Liu et al. [20] also found the same elements by Optical Emission Spectroscopy (OES), except potassium, in chemical composition of beverage cans with 1.08% Mg, 0.863% Mn, 0.589% Fe and 0.18% Si. However, they only used Coca-Cola™ cans in their studies whereas in this work different soda and beer cans were used, which justifies the differences in the obtained values. Also, although those authors did not identify potassium in beverage cans, its presence together with that of other alkaline metal salts is common in printing ink applied on surface of food and beverage cans, in order to increase the electroconductivity, as revealed by Fujisawa [22].

After alumina preparation and its impregnation with nickel, the same elements present in AL-T were identified by XRF in sample AS-T 10N, besides the nickel, as show Table 1 data. For AS 10N sample, only iron, magnesium, manganese, and silicon were identified, potassium not being detected. Each element content was under 2%, lower than that identified in AL-T, probably due to its elimination during the precipitation, washing and calcination steps used during the catalyst synthesis procedures.

Ni and Al contents in a stoichiometric nickel aluminate ($NiAl_2O_4$) are about 52 and 48 wt%, respectively. XRF results shown in Table 1 point out the presence of stoichiometric nickel aluminate in sample AC 10 N, but non-stoichiometric nickel aluminate in AS-T 10 N and AS 10 N samples. It was also possible to observe that nickel contents decreased in materials based on aluminum cans powders (AS-T 10N and AS 10N) when compared to the

Table 1 Chemical composition, determined by XRF, of aluminum cans powders with ink (AL-T) and of aluminas impregnated with 10 wt% Ni (AS-T 10N, AS 10N and AC 10N)

Sample	Weight %							
	Al	Ni	Fe	Mg	Mn	K	Si	Others
AL-T	92.8	–	1.18	3.30	1.34	0.68	0.59	0.15
AS-T 10N	50.2	44.8	1.97	1.29	0.95	0.53	0.13	0.13
AS 10N	48.0	48.1	1.02	1.71	0.83	–	0.13	0.12
AC 10N	47.6	52.2	–	–	–	–	–	0.02

sample obtained by conventional method (AC 10N), probably due to the substitution of Ni in the spinel structure by the other metals (Fe, Mg, Mn or K). Such contaminants can act as dopants, modifying catalyst properties, such as specific area, nickel reducibility, metallic dispersion and, consequently, catalytic activity. Despite the presence of contaminants in the calcined materials, their oxides were not detected by XRD due to their low contents.

3.3 SEM

Also, it was possible to notice from SEM images (Fig. 2) that, after impregnation, AS support surface became smoother and more uniform but with similar aspect to the one before impregnation. However, AC 10N morphology was different from AC support, presenting crackings on its surface. It may be related to nickel aluminate spinel

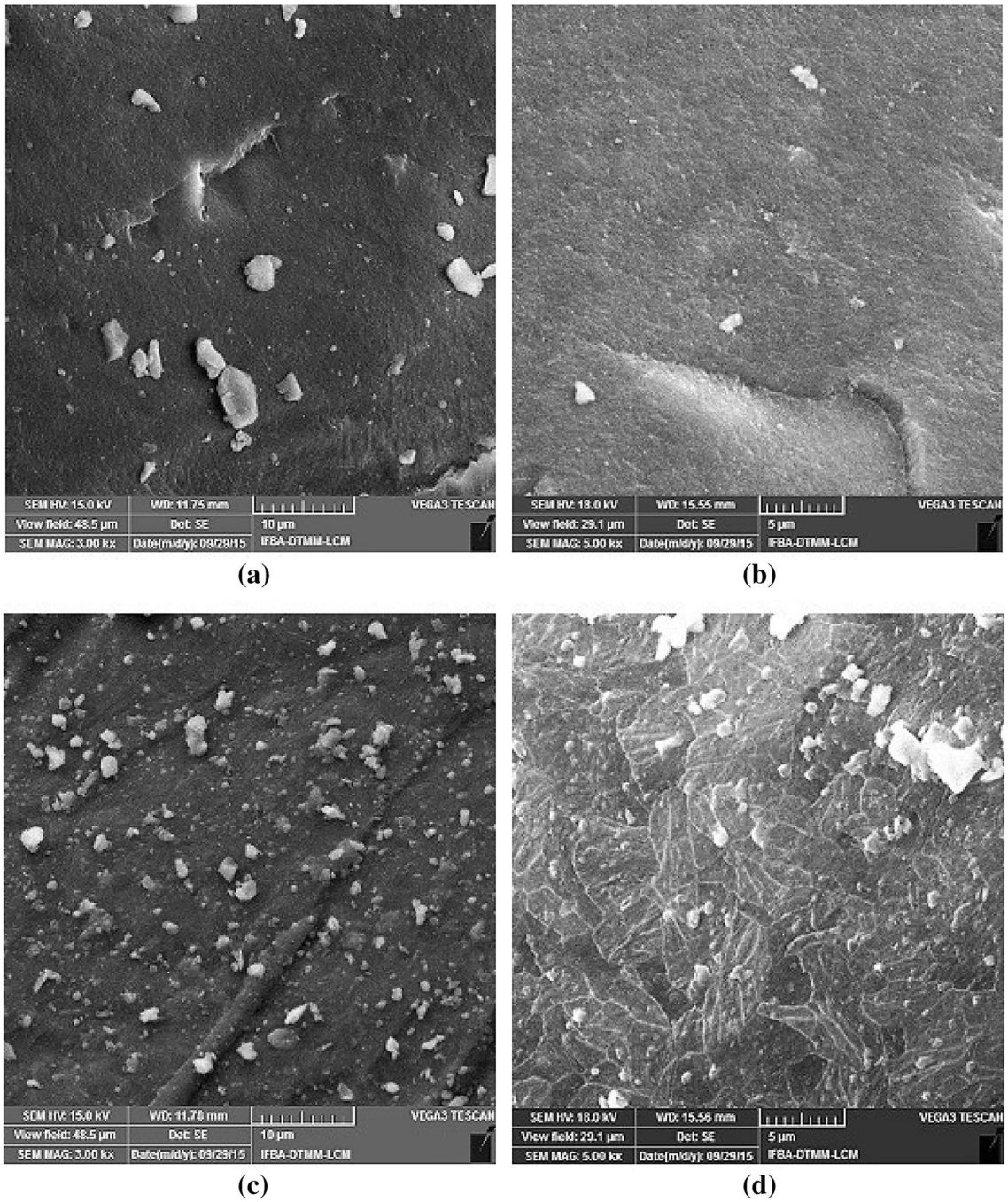

Fig. 2 Supports SEM images, AS (**a**) and AC (**c**), and supports impregnated with 10 wt% Ni, AS 10N (**b**) and AC 10N (**d**)

formation or higher nickel oxide segregation in this sample, as showed by XRD results.

3.4 Sg and Pv

Table 2 presents specific surface area (Sg) and pore volume (Pv) values for alumina without nickel and for alumina impregnated with nickel. It can be noticed that all alumina supports produced from aluminum cans powders, AS and AS-T, showed high specific surface area values. The specific area and pore volume values of that supports were similar to those of AC sample (203 $m^2\ g^{-1}$ and 0.32 $cm^3\ g^{-1}$, respectively) and higher than those of Cyanamid Ketjen CK 300 commercial alumina (180 $m^2\ g^{-1}$ and 0.5 $cm^3\ g^{-1}$, respectively), as reported in previous work [14]. It was also observed that AS-T specific surface area value was higher than those for AS or AC samples. Once potassium presence was detected in AS-T sample, as shown by XRF results, it is likely that the specific surface area increase is due to some promoter effect of this metal on the support. In fact, BET surface area increase for Ni/Al_2O_3-type catalysts when potassium is added as a promoter [23, 24].

After nickel addition (AS 10N, AS-T 10N and AC 10N samples), there was a decrease in the available specific surface area and in the pore volume, probably due to nickel aluminate spinel phase formation, detected by XRD, which shows lower specific surface area than alumina [25] or a pore volume decrease, as observed from Table 2 by alumina pores coverage with NiO particles deposited during the impregnation step [17, 26].

3.5 TPR

The profiles of temperature programmed reduction (Fig. 3) were similar, but the peaks appeared in different positions, indicating that different interaction types between the nickel oxides and the γ-alumina were obtained, depending on the preparation method. After the deconvolution of the profiles, three reduction zones were identified. The first one, with peaks in the range of 316–473 °C, was attributed to NiO reduction, free or segregated, in weak interaction with the support [27, 28], named α-NiO [29, 30]. The second zone, with maxima at 566, 601 and 613 °C, was associated with nickel oxide reduction in the vicinity of the alumina and strong interaction with the support [27], named β-NiO [29, 30]. The third zone starting at about 700 °C and with maxima in the range of 806–864 °C was related to nickel the reduction of aluminate structure [28, 31], which also constitutes one of the material phases detected by XRD. The nickel oxide in $NiO.Al_2O_3$ was classified as γ-NiO [29, 30]. In this zone, the peak at 702–748 °C may be related to the reduction of $NiAl_2O_4$ large particles, while the one in the range of 805–864 °C is attributed to the reduction of smaller size aluminate particles. The peaks of the third zone showed higher intensity than those of the first or second ones, indicating that most of the nickel is in strong interaction with alumina forming the spinel structure. This contributes to higher metal dispersion on the support.

The shift of the peaks from these zones to lower temperatures for AS-T 10N profile indicated weaker nickel-support interaction in this sample when compared to the others. This fact may be related to the presence potassium in AS-T 10N sample, which comes from the can ink, as identified by XRF analysis. According to the literature [21, 32], potassium can act as a promoter on Ni/Al_2O_3 catalysts, because it modifies the interaction between nickel oxide particles and the support and, as a consequence, favors the reduction by H_2 of nickel species. Table 3 shows the total hydrogen consumption values for the three samples calculated from areas under TPR peaks. The theoretical value was determined from the assumption of NiO to Ni^0 complete reduction. Also, the relative amount of reduced nickel species (α-NiO, β-NiO and γ-NiO) was also calculated; the values are shown in Table 3. According to hydrogen consumption values, indicated in Table 3, all nickel species were reduced for AS 10N and AC 10N catalysts and a smaller amount of nickel species was reduced for the sample obtained from cans with ink (AS-T 10N). Probably, although potassium has somewhat eased the reduction of a nickel species fraction, part of it can give a compound from its interaction with nickel oxide and alumina that it would be difficult to be reduced with H_2 and would not be identified by XRD,. On the other hand, more nickel species were reduced for AS 10N and AC 10N samples. For both samples, a higher amount of metallic nickel should be available to act as the active phase during the reactions whereas the opposite should occur with AS-T 10N catalyst.

It was also noted that a larger amount of free nickel oxide (α-NiO) was reduced for AS-T 10N and AS 10N samples while more β-NiO species were present in AC 10N sample. This is in agreement with XRD results, in which reflections were detected due to the segregated nickel oxide in samples prepared from aluminum cans powders (AS-T 10N and AS 10N), but there were no clear peaks related

Table 2 Samples specific surface area (Sg) and pore volume (Pv)

Sample	Sg ($m^2\ g^{-1}$)	Pv ($cm^3\ g^{-1}$)
AS-T	231.6 ± 1.1	0.36
AS	203.8 ± 1.5	0.35
AC	202.8 ± 0.6	0.32
AS-T 10N	143.1 ± 1.7	0.27
AS 10N	135.2 ± 0.4	0.27
AC 10N	134.6 ± 0.5	0.27

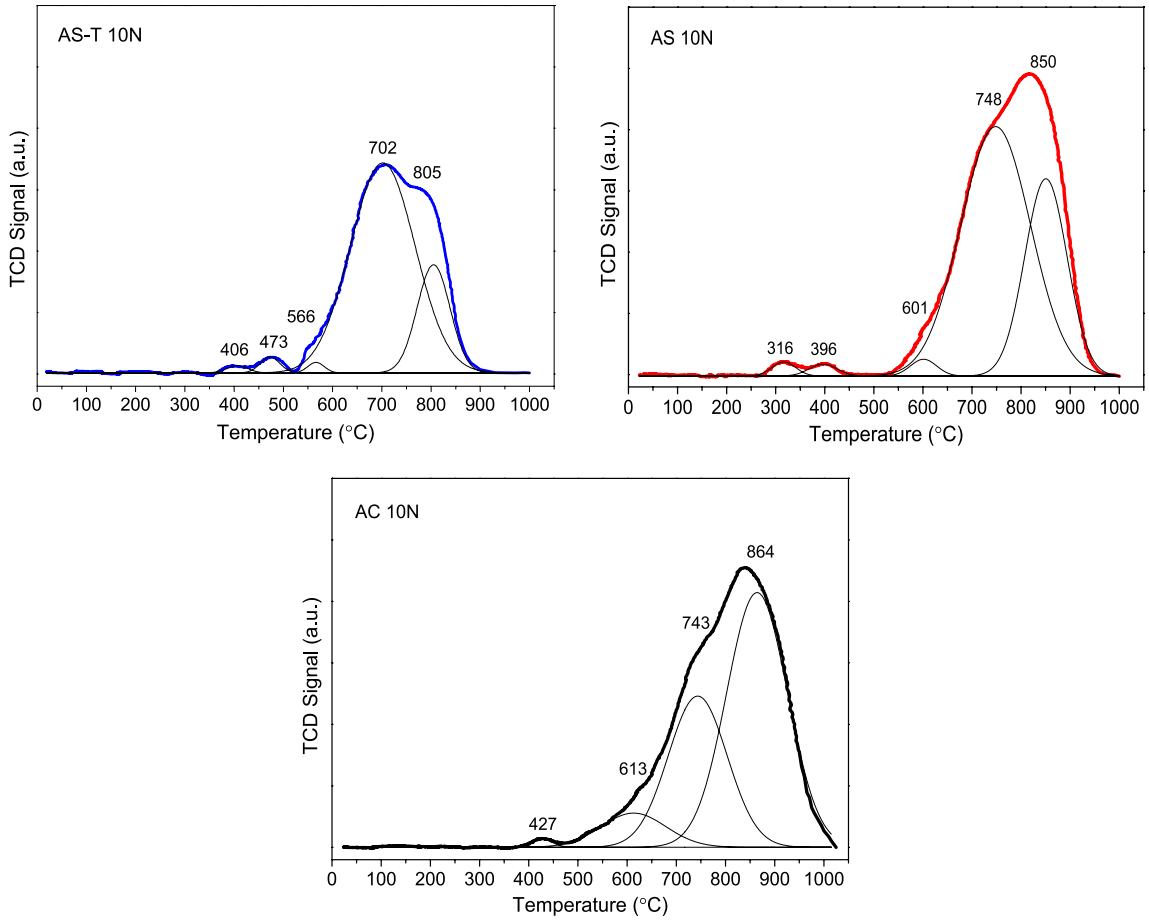

Fig. 3 Catalysts TPR profiles

Table 3 Values of H_2 consumption and the relative amount of Ni reduced species obtained from samples TPR profiles

Catalyst	H_2 consumption (mmol g^{-1})		Relative amount of Ni reduced species(%)		
	Theoretical	Experimental	α	β	γ
AS-T 10N	1.9	1.4	3.1	1.3	95.6
AS 10N	1.9	2.2	2.8	1.8	95.4
AC 10N	1.9	2.2	0.8	8.4	90.8

to free NiO in the sample obtained by conventional co-precipitation method (AC 10 N) due to NiO–Al_2O_3 (β-NiO) interaction which led to NiO and $NiAl_2O_4$ overlapping of peaks. The number of reducible γ-NiO species was lower in the AC 10 N sample (90.8%) when compared to the other samples where the amount corresponded to approximately 95% of the nickel oxide species.

Table 4 Reaction rate values (R°) and activation energy (Ea), determined from CHD, and methane conversion values (X_{CH4}), carbon dioxide conversion (X_{CO2}), hydrogen selectivity (S_{H2}) and H_2/CO ratio, obtained from MDR, after 5-h reaction

Catalyst	Ea (kcal mol^{-1})	R° (mol^{-1} g^{-1})	X_{CH4} (%)	X_{CO2} (%)	S_{H2} (%)	H_2/CO
AS 10N	19	0.37	80	90	83	0.72
AS-T 10N	27	0.17	68	79	82	0.68
AC 10N	22	0.17	72	75	80	0.68

3.6 CHD

The catalysts activation energy and reaction rate values for cyclohexane dehydrogenation are shown in Table 4. It can be observed that the activation energy was the lowest for AS 10N and, consequently, the reaction rate was higher with this catalyst when compared to the others. The cyclohexane dehydrogenation reaction was used to evaluate the metallic phase of the catalysts because it is a "non-demanding" one [33], this means that it does not require metal atoms specific arrangement to take place, and all sites have the same activity. The catalysts dehydrogenation activity evaluated from reaction rate values are, therefore, proportional to the total number of active sites exposed, that is, to their metallic dispersion.Thus, it is possible to conclude that Ni dispersion is higher for AS 10N catalyst than for the others. Besides, catalytic activity of AS 10N catalysts was showed to be better than AC 10N one due to aluminum can metals compounds, detected by XRF, which remained as part of the catalyst composition. Fe and Mn, for instance, when present as alumina-supported oxides exhibit activity in the cyclohexane dehydrogenation or in other dehydrogenation reactions [34–36].

Although AS-T 10N catalyst also has these metals in its composition, it showed higher activation energy and lower reaction rate than AS 10N catalyst. This can be explained considering the potassium effect on the AS-T 10N catalyst. When used as a promoter on nickel supported catalysts, some potassium content is in intimate contact with nickel whereas the remaining is distributed over the alumina support [37]. Several research works mentioned [23, 32, 38] that potassium can migrate from the support to nickel particles and be placed, predominantly, on their surface. In this way, K species can be placed over Ni, neutralizing a fraction of the active sites and, as a consequence, reducing the catalyst activity [23, 32, 37]. In this case, potassium effect seems to be more important than other metal contribution to increase the dehydrogenation activity. Thus, a decrease of the reaction rate of AS-T 10N catalyst compared to the one of AS 10 N is observed. Moreover, TPR results indicated that a smaller amount of nickel species was reduced in AS-T 10N sample which would also justify the lower catalyst dehydrogenation activity.

3.7 Catalytic Performance

The catalytic performance can be compared from the Table 4. All the catalysts showed high activity for methane dry reforming, with high CH_4 (68–80%) and CO_2 (75–90%) conversion, high selectivity to hydrogen (80–83%) and high H_2/CO ratio near to one (0.68–0.72), which makes its use feasible for industrial processes such as biogas reforming or similar reactions to obtain hydrogen and synthesis gas. It can be observed that in all cases CO_2 conversion was higher than CH_4 one, probably due to the secondary reverse water–gas shift reaction [21] in which CO_2 reacts with H_2, producing CO and H_2O. This fact also explains why H_2/CO molar ratio values, (Table 4) are lower than one and water production as by-product during the runs.

By comparing the conversion values with the different catalysts, it was noted that these varied in the following order: AS 10N > AS-T 10N ~ AC 10N. It means that metal traces such as Mg, Mn, Fe, K in AS 10N and AS-T 10N influences their catalytic activity for methane dry reforming and can improve it compared to the catalyst obtained by conventional method (AC 10N). There are many reports in the literature [21, 23, 32, 39] about Mg, Mn, and K promoter effect in nickel supported catalysts for dry reforming. Yong et al. [39] reported that alkaline metal oxides (Na_2O, K_2O) and alkaline earth metal oxides (CaO, MgO) enhance CO_2 adsorption on the metal oxide because CO_2 is an acidic gas and alkaline metals and alkaline earth metals oxides have basic character. So, these basic modifiers could suppress the coke deposition by the reaction of CO_2 with C to produce CO (reverse Boudouard reaction). Mn addition to Ni/Al_2O_3 catalysts produces a noticeable reduction in carbon deposition with a small decrease in catalytic activity, according to Choi et al. [40]. Luna and Iriarte [21] studied K-modified Ni/Al_2O_3 catalysts and observed that they showed low carbon content and high catalytic stability for 30-hour operation. They proved that addition of potassium in low amounts (0.5 wt%) to Ni/Al_2O_3 hinders coke accumulation on the catalyst surface, this being in agreement with the conclusions of other authors [23, 24, 32]. K also increases Ni species reducibility, probably by modifying the metal-support interaction, as mentioned in previous works [21, 32] and observed from TPR results. Unfortunately, Mg, Mn, and K improvement of the stability and decrease in coke deposition on Ni/Al_2O_3 catalysts used for methane dry reforming could not be verified from this research results because the operation time was much shorter than that the one used in the above mentioned works.

It was also proposed [21] that potassium migrates from the support to nickel surface and neutralizes a fraction of the most active sites for the reforming reaction producing, as a consequence, methane conversion decrease.This explains the CH_4 lower conversion showed by AS-T 10N compared to AS 10N. On the other hand, AS 10N catalyst best performance would be related to the increase in the activity of the metallic phase due to Fe and Mn, as previously discussed, or to the higher amount of reduced Ni available to the reaction which was identified by TPR.

4 Conclusions

In this work, the use of γ-alumina produced from aluminum can powders as support for Ni/γ-Al_2O_3 catalysts was investigated. Catalytic evaluation results showed that these systems are promising for methane dry reforming with high methane and carbon dioxide conversion, high selectivity to hydrogen and H_2/CO molar ratio close to 1, which makes their use feasible in industrial processes. Catalysts produced in this way are eco friendly for two reasons: (i) its usage for biogas reforming or other process which need renewable sources for hydrogen production, considered the future fuel, and synthesis gas which can be used to obtain chemical and fuels; (ii) its preparation route from a catalytic support obtained from recycling metal.

However, contaminants present in the carrier which come from aluminum can powders used for γ-Al_2O_3 preparation such as Mg, Mn, Fe, and K can affect catalyst properties and their performance for methane dry reforming in a favorable way. Nickel catalyst performance, prepared using γ-Al_2O_3 from aluminum can powders without ink, was better than that of nickel catalyst prepared using γ-Al_2O_3 obtained by conventional method or synthesized using aluminum can powders with ink. It could be attributed to nickel reducibility improvements, nickel-support interaction, nickel dispersion and metallic phase activity in the presence of Mg, Mn, and Fe. On the other hand, despite the K effects on increasing the specific surface area and modifying nickel oxide and support interaction, easing the reduction of a fraction nickel species, that metal also covers and neutralizes the most active nickel sites for methane dry reforming. As a consequence, it contributes to the activity decrease of nickel catalyst supported on alumina obtained from aluminum can powders with ink, where it is present.

In summary, the use of alumina produced from aluminum recycling to obtain Ni/Al_2O_3 catalysts for methane dry reforming or biogas dry reforming is very interesting since the support has metallic promoters that are not necessary to be added during the preparation step. It can be advantageous, both economically and environmentally.

Acknowledgements The authors would like to thank Pró-Reitoria de Pesquisa, Pós-graduação e Inovação do Instituto Federal da Bahia PRPGI-IFBA (Brazil) for the grants issued to YFA and LSC, Universidad Nacional del Litoral—UNL and Consejo Nacional de Investigaciones Científicas y Técnicas—CONICET (Argentina) for the financial assistance to ADB, Antonia Soares (UNEB, Brazil) for XRD analyzes, Carina Soares (DTMM-LCM/IFBA, Brazil) for SEM analysis, LABTAM (UFRN, Brazil) for TPR analyzes and PPGCEM/UFRN for XRF analysis.

References

1. Alonso DM, Bond JQ, Dumesic JA (2010) Green Chem 12:1493–1513
2. Courson C, Udron L, Swierczynski D, Petit C, Kiennemann A (2002) Catal Today 76:75–86
3. Fatsikostas AN, Kondarides D, Verykios XE (2002) Catal Today 75:145–155
4. Kondarides DI, Daskalaki VM, Patsoura A, Verykios XE (2008) Catal Lett 122:26–32
5. Damyanova S, Pawelec B, Arishtirova K, Fierro JLG (2011) Int J Hydrog Energy 36:10635–10647
6. Chen G, Yao J, Liu J, Yan B, Shan R (2016) Renew. Energy 91:315–322
7. Yang J, Kaewpanha M, Karnjanakom S, Guan G, Hao X, Abudula A (2016) Int J Hydrog Energy 41:6699–6705
8. Al–Fatish ASA, Ibrahim AA, Fakeeha AH, Soliman MA, Siddiqui MRH, Abasaeed AE (2009) Appl Catal A 364:150–155
9. Rathod V, Bhale P (2014) Energy Procedia 54:236–245
10. Melo F, Morlanés N (2005) Catal Today 107:458–466
11. Rathod VP, Shete J, Bhale PV (2016) Int J Hydrog Energy 41:132–138
12. Charisiou ND, Siakavelas G, Papageridis KN, Baklavaridis A, Tzounis L, Avraam DG, Goula MA (2016) J Nat Gas Sci Eng 31:164–183
13. Constantino VRL, Araki K, Silva DO, Oliveira W (2002) Quím. Nova 25:490–498
14. Adans YF, Martins AR, Coelho RE, Virgens CF, Ballarini AD, Carvalho LS (2016) Mater Res 19:977–982
15. Balakrishnan M, Batra VS, Hargreaves JSJ, Pulford ID (2011) Green Chem 13:16–24
16. Coelho RE (2015) Brazilian Patent PI 1106612-1 A2
17. Asencios YJO, Elias KFM, Assaf EM (2014) Appl Surf Sci 317:350–359
18. Lo Jacono M, Schiavello M, Cimino A (1971) J Phys Chem A 75:1044–1050
19. Sanchez EA, Comelli RA (2014) Int J Hydrog Energy 39:8650–8655
20. Liu W, Niu T, Yang J, Wang Y, Hu S, Dong Y, Xu H (2011) Micro Nano Lett 6:852–854
21. Luna AEC, Iriarte ME (2008) Appl Catal A 343:10–15
22. Fujisawa T (1992) US Patent 5087659 A
23. Nagaraja BM, Bulushev DA, Beloshapkin S, Ross JRH (2011) Catal Today 178:132–136
24. Siahvashi A, Adesina AA (2013) Catal Today 214:30–41
25. Guo J, Lou H, Zhao H, Chai D, Zheng X (2004) Appl Catal A 273:75–82
26. Lima SP, Vicentini V, Fierro JLG, Rangel MC (2008) Catal Today 135:925–930
27. Pawelec B, Damyanova S, Arishtirova K, Fierro JLG, Petrovet L (2007) Appl Catal A 323:188–201
28. Rahmani S, Rezaei M, Meshkani F (2014) J Ind Eng Chem 20:1346–1352
29. Boukha Z, Jiménez-González C, Rivas B, González-Velasco JR, Gutiérrez-Ortiz JI, López-Fonseca R (2014) Appl Catal B 158–159:190–201
30. Boukha Z, Jiménez-González C, Gil-Calvo M, Rivas B, González-Velasco JR, Gutiérrez-Ortiz JI, López-Fonseca R (2016) Appl Catal B 199:372–383
31. López-Fonseca R, Jiménez-González C, Rivas B, Gutiérrez-Ortiz JI (2012) Appl Catal A 437–438:53–62
32. Juan-Juan J, Román Martínez MC, Illán-Gómez MJ (2006) Appl Catal A 301:9–15
33. Boudart M, Aldag A, Benson JE, Dougharty NA, Harkins CG (1996) J Catal 6:92–99

34. Richardson PC, Rossington DR (1969) J Catal 14:175–181
35. Al-Zahrani SM, Jibril BY, Abasaeed AE (2003) Catal Lett 85:57–67
36. Sun Y, Wu Y, Tao L, Shan H, Wang G, Li C (2015) J Mol Catal A 397:120–126
37. Borowiecki T, Denis A, Rawski M, Gołębiowski A, Stołecki K, Dmytrzyk J, Kotarba A (2014) Appl Surf Sci 300:191–200
38. Snoeck W, Froment GF (2002) Ind Eng Chem Res 41:3548–3556
39. Yong Z, Mata V, Rodrigues AE (2002) Sep Purif Technol 26:195–205
40. Choi JS, Moon KI, Kim YG, Lee JS, Kim CH, Trimm DL (1998) Catal Lett 52:43–47